ZEUS-prel-05-026

Submitted to the
XXXIII International Conference on High Energy Physics
July 26 - August 2, 2006, Moscow, Russia

Abstract: 13 **Session: QCD hard interactions**

Angular correlations in three-jet production in deep inelastic scattering at HERA

ZEUS Collaboration

Abstract

Three-jet production in deep inelastic *ep* scattering has been investigated with the ZEUS detector at HERA using an integrated luminosity of 81.7 pb^{-1}. Jets were identified using the k_T cluster algorithm in the longitudinally invariant inclusive mode in the Breit frame. Angular correlations between the three jets in the final state and the proton beam direction were investigated to separate the contributions from the different color configurations. The measurements are compared to fixed-order perturbative calculations assuming the values of the colour factors C_F, C_A and T_F as derived from a variety of gauge groups.

1 Introduction

Quantum chromodynamics (QCD), the gauge theory of the strong interactions which acts on the quark-fermion fields, is based on the SU(3) non-abelian group, which induces the self-coupling of the gauge bosons, the gluons. Investigations of the triple-gluon vertex have been carried out at LEP [1, 2] using angular correlations in four-jet events from Z^0 hadronic decays.

At HERA, the effects of the different color configurations arising from the underlying gauge structure have been studied in three-jet events in direct photoproduction [3]. Neutral current (NC) deep inelastic scattering (DIS) events also provide a clean way to study the effects of the different color configurations. An illustrative diagram for each color configuration is shown in Fig. 1: (A) double-gluon bremsstrahlung from a quark line (proportional to C_F^2), (B) the splitting of a virtual gluon into a pair of final-state gluons (proportional to $C_F C_A$), (C) the production of a $q\bar{q}$ pair through the exchange of a virtual gluon emitted by an incoming quark (proportional to $C_F T_F$) and (D) the production of a $q\bar{q}$ pair through the exchange of a virtual gluon arising from the splitting of an incoming gluon (proportional to $T_F C_A$). The variables that have been devised to distinguish the contributions from the different color configurations make use only of the three highest-$E_T^{\rm jet}$ jets in an event and are:

- $\boldsymbol{\theta_H}$, the angle between the plane determined by the highest transverse energy jet and the beam and the plane determined by the two lowest transverse energy jets [4];
- $\boldsymbol{\alpha_{23}}$, which is inspired by the variable $\alpha_{34}^{e^+e^-}$ [2] for $e^+e^- \to 4$ jets, is defined as the angle between the two lowest transverse energy jets;
- $\boldsymbol{\beta_{\rm KSW}}$, which is inspired by the Körner-Schierholz-Willrodt angle $\Phi_{\rm KSW}^{e^+e^-}$ [5] for $e^+e^- \to$ 4 jets, is defined as
$$\cos(\beta_{\rm KSW}) = \cos\left[\tfrac{1}{2}\left(\angle[(\vec{p}_1 \times \vec{p}_3),(\vec{p}_2 \times \vec{p}_B)] + \angle[(\vec{p}_1 \times \vec{p}_B),(\vec{p}_2 \times \vec{p}_3)]\right)\right],$$
where $\vec{p}_i,\ i = 1, ..., 3$ is the momentum of jet i and $\vec{p}_B$ is a unit vector in the direction of the beam; the jets are ordered according to decreasing transverse energy;
- $\boldsymbol{\eta_{\rm max}^{\rm jet}}$, the maximum pseudorapidity of the three jets with highest transverse energy.

In e^+e^- annihilation into four-jet events, the distribution of $\Phi_{\rm KSW}^{e^+e^-}$ is sensitive to the differences between $q\bar{q}gg$ and $q\bar{q}q\bar{q}$ final states whereas that of $\alpha_{34}^{e^+e^-}$ distinguishes between contributions from double-bremsstrahlung diagrams and diagrams involving the triple-gluon coupling. For three-jet events in ep interactions, the variable θ_H is sensitive to the triple-gluon coupling in quark-induced processes (see Fig. 1B).

Three-jet cross sections have been measured previously in NC DIS [6]. The measured cross sections are well reproduced by perturbative QCD calculations and a value of the strong coupling constant, α_s, was extracted. In this paper, measurements of the angular distributions sensitive to the contributions from the different color configurations are presented and compared to fixed-order $\mathcal{O}(\alpha\alpha_s^2)$ perturbative calculations.

2 Experimental set-up

A detailed description of the ZEUS detector can be found elsewhere [7,8]. A brief outline of the components that are most relevant for this analysis is given below.

Charged particles are tracked in the central tracking detector (CTD) [9], which operates in a magnetic field of 1.43 T provided by a thin superconducting solenoid. The CTD consists of 72 cylindrical drift-chamber layers, organized in nine superlayers covering the polar-angle[1] region $15^\circ < \theta < 164^\circ$. The transverse-momentum resolution for full-length tracks can be parameterised as $\sigma(p_T)/p_T = 0.0058 p_T \oplus 0.0065 \oplus 0.0014/p_T$, with p_T in GeV. The tracking system was used to measure the interaction vertex with a typical resolution along (transverse to) the beam direction of 0.4 (0.1) cm and to cross-check the energy scale of the calorimeter.

The high-resolution uranium–scintillator calorimeter (CAL) [10] covers 99.7% of the total solid angle and consists of three parts: the forward (FCAL), the barrel (BCAL) and the rear (RCAL) calorimeters. Each part is subdivided transversely into towers and longitudinally into one electromagnetic section (EMC) and either one (in RCAL) or two (in BCAL and FCAL) hadronic sections (HAC). The smallest subdivision of the calorimeter is called a cell. Under test-beam conditions, the CAL single-particle relative energy resolutions were $\sigma(E)/E = 0.18/\sqrt{E}$ for electrons and $\sigma(E)/E = 0.35/\sqrt{E}$ for hadrons, with E in GeV.

The luminosity was measured from the rate of the bremsstrahlung process $ep \rightarrow e\gamma p$. The resulting small-angle energetic photons were measured by the luminosity monitor [11], a lead-scintillator calorimeter placed in the HERA tunnel at $Z = -107$ m.

[1] The ZEUS coordinate system is a right-handed Cartesian system, with the Z axis pointing in the proton beam direction, referred to as the "forward direction", and the X axis pointing left towards the centre of HERA. The coordinate origin is at the nominal interaction point.

3 Data selection and jet search

The data were collected during the running period 1998-2000, when HERA operated with protons of energy $E_p = 920$ GeV and electrons or positrons[2] of energy $E_e = 27.5$ GeV, and correspond to an integrated luminosity of 81.7 ± 1.9 pb^{-1}.

Neutral current DIS events were selected offline using criteria similar to those reported previously [12]. The main steps are listed below.

The scattered-electron candidate was identified from the pattern of energy deposits in the CAL [13]. The energy (E'_e) and polar angle (θ_e) of the electron candidate were determined from the CAL measurements. The Q^2 variable was reconstructed from the double angle method ($Q^2_{\rm DA}$) [14], which uses θ_e and the angle γ_h, which corresponds, in the quark-parton model, to the direction of the scattered quark. The angle γ_h was reconstructed from the CAL measurements of the hadronic final state [14]. The following requirements were imposed on the data sample:

- an electron candidate of energy $E'_e > 10$ GeV;
- $y_e < 0.95$, where $y_e = 1 - E'_e(1 - \cos\theta_e)/(2E_e)$;
- the total energy not associated with the electron candidate within a cone of radius 0.7 units in the pseudorapidity-azimuth ($\eta - \varphi$) plane around the electron direction should be less than 10% of the electron energy;
- for $30^\circ < \theta_e < 140^\circ$, the fraction of the electron energy within a cone of radius 0.3 units in the $\eta - \varphi$ plane around the electron direction should be larger than 0.9; for $\theta_e < 30^\circ$, the cut was raised to 0.98;
- the vertex position along the beam axis should be in the range $|Z| < 34$ cm;
- $38 < (E - p_Z) < 65$ GeV, where E is the total energy as measured by the CAL, $E = \sum_i E_i$, and p_Z is the Z-component of the vector $\boldsymbol{p} = \sum_i E_i \boldsymbol{r_i}$; in both cases the sum runs over all CAL cells, E_i is the energy of the CAL cell i and $\boldsymbol{r_i}$ is a unit vector along the line joining the reconstructed vertex and the geometric centre of the cell i;
- $p_T^{\rm miss}/\sqrt{E_T} < 2.5$ GeV$^{1/2}$, where $p_T^{\rm miss}$ is the missing transverse momentum as measured with the CAL ($p_T^{\rm miss} \equiv \sqrt{p_X^2 + p_Y^2}$) and E_T is the total transverse energy in the CAL;
- the event is rejected if there is a second electron candidate with energy above 10 GeV and the total energy in the CAL, after subtracting that of the two electron candidates, is below 4 GeV;
- $Q^2_{\rm DA} > 125$ GeV^2;

[2] Here and in the following, the term "electron" denotes generically both the electron (e^-) and the positron (e^+), unless otherwise stated.

- $|\cos\gamma_h| < 0.65$.

The k_T cluster algorithm [15] was used in the longitudinally invariant inclusive mode [16] to reconstruct jets in the hadronic final state both in data and in Monte Carlo (MC) simulated events (see Section 4). In data, the algorithm was applied to the energy deposits measured in the CAL cells after excluding those associated with the scattered-electron candidate. The jet search was performed in the $\eta - \varphi$ plane of the Breit frame. The jet variables were defined according to the Snowmass convention [17].

After reconstructing the jet variables in the Breit frame, the massless four-momenta were boosted into the laboratory frame, where the transverse energy ($E^{\rm jet}_{\rm T,LAB}$) and the pseudorapidity ($\eta^{\rm jet}_{\rm LAB}$) of each jet were calculated. Energy corrections were then applied to the jets in the laboratory frame and propagated into the jet transverse energy in the Breit frame, $E^{\rm jet}_{T,{\rm B}}$. The jet variables in the laboratory frame were also used to apply additional cuts on the selected sample:

- events were removed from the sample if the distance of any of the jets to the electron candidate in the $\eta - \varphi$ plane of the laboratory frame, was smaller than 1 unit;
- events were removed from the sample if any of the jets was in the backward region of the detector ($\eta^{\rm jet}_{\rm LAB} < -2$);
- jets with low transverse energy in the laboratory frame ($E^{\rm jet}_{\rm T,LAB} < 2.5$ GeV) were not included in the final sample;

The jets in the Breit frame were ordered in transverse energy. The final data sample contained 1015 events with at least three jets satisfying $E^{\rm jet1}_{T,{\rm B}} > 8$ GeV, $E^{\rm jet2,3}_{T,{\rm B}} > 5$ GeV and $-2 < \eta^{\rm jet}_{\rm B} < 1.5$, where $\eta^{\rm jet}_{\rm B}$ is the jet pseudorapidity in the Breit frame.

4 Monte Carlo simulation

Samples of events were generated to determine the response of the detector to jets of hadrons and the correction factors necessary to obtain the hadron-level jet cross sections. The generated events were passed through the GEANT 3.13-based [18] ZEUS detector- and trigger-simulation programs [8]. They were reconstructed and analysed by the same program chain as the data.

Neutral current DIS events including radiative effects were simulated using the HERACLES 4.6.1 [19] program with the DJANGOH 1.1 [20] interface to the hadronisation programs. HERACLES includes corrections for initial- and final-state radiation, vertex and propagator terms, and two-boson exchange. The QCD cascade is simulated using the colour-dipole model (CDM) [21] including the leading-order (LO) QCD diagrams as implemented in ARIADNE 4.08 [22] and, with the MEPS model of LEPTO 6.5 [23]. The

CTEQ5D [24] proton PDFs were used for these simulations. Fragmentation into hadrons is performed using the Lund string model [25] as implemented in Jetset [26, 27]

The jet search was performed on the MC events using the energy measured in the CAL cells in the same way as for the data. Using the sample of events generated with either Ariadne or Lepto-MEPS and after applying the same offline selection as for the data, a reasonably good description of the measured distributions for the kinematic and jet variables was found. The average between the acceptance correction values obtained with Ariadne and Lepto-MEPS was used to correct the data to the hadron level. The same jet algorithm was also applied to the hadrons (partons) to obtain the predictions at the hadron (parton) level.

5 Fixed-order calculations

The leading-order (LO) calculation of three-jet cross sections in NC DIS can be expressed in terms of the color factors C_A, C_F and T_F as follows:

$$\sigma_{ep\to 3\text{jets}} = C_F^2 \cdot \sigma_A + C_F C_A \cdot \sigma_B + C_F T_F \cdot \sigma_C + T_F C_A \cdot \sigma_D, \tag{1}$$

where $\sigma_A, ..., \sigma_D$ are the partonic cross sections for the different contributions (see Fig. 1). The C_F, C_A and T_F color factors are the physical manifestation of the underlying group structure. In strong interactions, they represent the relative strengths of the processes $q \to qg$, $g \to gg$ and $g \to q\bar{q}$, respectively.

The calculations of $\sigma_A, ..., \sigma_D$ used in this analysis are based on the program Disent [28]. The calculations were performed in the $\overline{MS}$ renormalisation and factorisation schemes using a generalised version [28] of the subtraction method [29]. The number of flavours was set to five and the renormalisation (μ_R) and factorisation (μ_F) scales were chosen to be $\mu_R = \mu_F = Q$. The strong coupling constant, α_s, was calculated at two loops with $\Lambda^{(5)}_{\overline{MS}} = 226$ MeV, corresponding to $\alpha_s(M_Z) = 0.118$. The calculations were performed using the CTEQ6 [30] parameterisations of the proton PDFs. These calculations are $\mathcal{O}(\alpha\alpha_s^2)$ and represent the lowest-order contribution to three-jet events in NC DIS.

Since the measurements refer to jets of hadrons, whereas the calculations refer to jets of partons, the predictions were corrected to the hadron level using the MC models. The multiplicative correction factor (C_{had}) was defined as the ratio of the cross section for jets of hadrons over that for jets of partons, estimated by using the MC programs described in Section 4. The normalised cross-section calculations changed typically by less than $\pm 10\%$ upon application of the parton-to-hadron corrections. Other effects not accounted for in the calculations, namely QED radiative corrections and Z^0 exchange, were found to be very small for the normalised cross-section calculations and, therefore, neglected.

6 Systematic uncertainties

The following sources of systematic uncertainty were considered for the measured jet cross sections:

- the uncertainty in the absolute energy scale of the jets was estimated to be $\pm 1\%$ for $E^{\rm jet}_{\rm T,LAB} > 10$ GeV and $\pm 3\%$ for lower $E^{\rm jet}_{\rm T,LAB}$ values [31];
- the uncertainty in the absolute energy scale of the electron candidate was estimated to be $\pm 1\%$ [32];
- the deviations in the results obtained by using either ARIADNE or LEPTO-MEPS to correct the data from their average, were taken to represent systematic uncertainties;
- the $E^{\rm jet}_{\rm T,LAB}$ cut was raised to 4 GeV;
- the cut in $\eta^{\rm jet}_{\rm LAB}$ used to suppress the contamination due to photons falsely identified as jets in the Breit frame was set to -3 and to -1.5;
- the uncertainty in the simulation of the trigger.

The effect of these uncertainties on the normalised cross sections is small compared to the statistical uncertainties for the measurements presented in Section 7. The systematic uncertainties were added in quadrature to the statistical uncertainties and are shown in the figures as error bars.

7 Results

Using the selected data sample, normalised three-jet differential cross sections were measured for $Q^2 > 125$ GeV^2 and $|\cos\gamma_h| < 0.65$. The cross sections were determined for inclusive three-jet events with $E^{\rm jet1}_{T,{\rm B}} > 8$ GeV, $E^{\rm jet2,3}_{T,{\rm B}} > 5$ GeV and $-2 < \eta^{\rm jet}_{\rm B} < 1.5$.

The cross-sections $(1/\sigma)(d\sigma/d\theta_H)$ and $(1/\sigma)(d\sigma/d\cos\alpha_{23})$ are presented in Figs. 2a and 2b, respectively. The measured cross section as a function of $\cos\alpha_{23}$ peaks around 0.4; $(1/\sigma)(d\sigma/d\theta_H)$ increases as θ_H increases. Figure 2c shows the normalised cross section as a function of $\cos\beta_{\rm KSW}$. The normalised cross section as a function of $\eta^{\rm jet}_{\rm max}$ is presented in Fig. 2d; the measured cross section increases as $\eta^{\rm jet}_{\rm max}$ increases.

Leading-logarithm parton-shower Monte Carlo calculations using either MEPS or CDM are compared to the data in Fig. 2. The fractional difference between the measured normalised cross section and the corresponding predictions of the models are shown in the lower part of Figs. 2(a)-(d). The predictions of MEPS give a good description of the data, whereas those from CDM give a somewhat poorer description of the measured normalised cross sections.

Fixed-order calculations of the individual color components from Eq. 1 are compared to the data in Fig. 3. The predicted relative contributions by SU(3) are A: 23%, B: 13%, C: 39% and D: 25%. Therefore, the contribution from diagrams that involve the triple-gluon coupling amounts to 38% in SU(3). The component which contains the contribution from the triple-gluon vertex in quark-induced processes (Fig. 1B), σ_B, has a different shape than the other components for θ_H, $\cos\alpha_{23}$ and $\cos\beta_{\rm KSW}$, but its contribution in SU(3) is small. The component with the triple-gluon vertex in Fig. 1D, σ_D, has a shape which is very similar to that of Fig. 1A for these variables and it is best distinguished by the $\eta^{\rm jet}_{\rm max}$ distribution. Therefore, the three-jet angular variables studied are sensitive to the different color configurations. The full calculation, in which each contribution has been weighted according to the color factors predicted by SU(3), is compared to the data in Fig. 4. These calculations give a reasonable description of the data for all angular observables.

To illustrate the sensitivity of the measurements to the color factors, calculations based on different symmetry groups are also compared to the data in Fig. 4. In this figure, the color components have been combined in such way as to reproduce the color structure of a theory based on the non-abelian group SU(N) in the limit of large N ($C_F = (N^2-1)/2N, T_F = 1/2, C_A = N$), the abelian group U(1)^3 ($C_F = 1, T_F = 3, C_A = 0$) and, as an extreme choice, a calculation with $C_F = 0$, $T_F = 1/2$ and $C_A = 3$. The predictions of U(1)^3 show differences of around 10% with respect to those of SU(3), which are of the same order as the statistical uncertainties. As can be seen from Fig. 4, the data clearly disfavour a theory in which $T_F/C_F \approx 0$ such as predicted by SU(N) in the limit of large N or $C_F = 0$.

8 Summary

Measurements of angular correlations in three-jet events in NC DIS have been made in ep collisions using 81.7 pb^{-1} of data collected with the ZEUS detector at HERA. The cross sections refer to jets identified in the Breit frame with the longitudinally invariant k_T cluster algorithm in the inclusive mode and selected with $E^{\rm jet1}_{T,{\rm B}} > 8$ GeV, $E^{\rm jet2,3}_{T,{\rm B}} > 5$ GeV and $-2 < \eta^{\rm jet}_{\rm B} < 1.5$. The measurements were made in the kinematic region defined by $Q^2 > 125$ GeV^2 and $|\cos\gamma_h| < 0.65$.

Normalised differential cross sections were measured as functions of θ_H, α_{23}, $\beta_{\rm KSW}$ and $\eta^{\rm jet}_{\rm max}$. Fixed-order ($\mathcal{O}(\alpha\alpha_s^2)$) calculations for three-jet events in NC DIS separated according to the color configurations were used to study the sensitivity of the angular distributions to the underlying gauge structure. The predicted distributions of θ_H, α_{23} and $\beta_{\rm KSW}$ distinguish well the contribution from the triple-gluon coupling in quark-induced processes and $\eta^{\rm jet}_{\rm max}$ distinguishes the contribution coming from gluon induced processes.

The measurements are found to be consistent with the admixture of color configurations as predicted by SU(3). The data clearly disfavour a theory in which $T_F/C_F \approx 0$, as predicted by SU(N) in the limit of large N, or $C_F = 0$.

Acknowledgements

We thank the DESY Directorate for their strong support and encouragement. The remarkable achievements of the HERA machine group were essential for the successful completion of this work and are greatly appreciated.

References

[1] ALEPH Coll., R. Alemany et al., Phys. Lett. **B 284**, 151 (1992);
ALEPH Coll., R. Barate et al., Z. Phys. **C 76**, 1 (1997);
ALEPH Coll., A. Heister et al., Eur. Phys. J. **C 27**, 1 (2003);
DELPHI Coll., P. Abreu et al., Z. Phys. **C 59**, 357 (1993);
DELPHI Coll., P. Abreu et al., Phys. Lett. **B 414**, 401 (1997);
DELPHI Coll., P. Abreu et al., Phys. Lett. **B 449**, 383 (1999);
L3 Coll., B. Adeva et al., Phys. Lett. **B 248**, 227 (1990);
OPAL Coll., M.Z. Akrawy et al., Z. Phys. **C 49**, 49 (1991);
OPAL Coll., R. Akers et al., Z. Phys. **C 65**, 367 (1995);
OPAL Coll., G. Abbiendi et al., Eur. Phys. J. **C 20**, 601 (2001).

[2] DELPHI Coll., P. Abreu et al., Phys. Lett. **B 255**, 466 (1991).

[3] ZEUS Coll., *Study of color dynamics in photoproduction at HERA*. Abstract 5-0271, 32nd International Conference on High Energy Physics, Beijing, China, 2004.

[4] R. Muñoz-Tapia and W.J. Stirling, Phys. Rev. **D 52**, 3894 (1995).

[5] J.G. Körner, G. Schierholz and J. Willrodt, Nucl. Phys. **B 185**, 365 (1981).

[6] ZEUS Coll., S. Chekanov et al., Preprint DESY-05-019 (hep-ex/0502007), DESY, 2005;
H1 Coll., C. Adloff et al., Phys. Lett. **B 515**, 17 (2001).

[7] ZEUS Coll., M. Derrick et al., Phys. Lett. **B 293**, 465 (1992).

[8] ZEUS Coll., U. Holm (ed.), *The ZEUS Detector*. Status Report (unpublished), DESY (1993), available on `http://www-zeus.desy.de/bluebook/bluebook.html`.

[9] N. Harnew et al., Nucl. Inst. Meth. **A 279**, 290 (1989);
B. Foster et al., Nucl. Phys. Proc. Suppl. **B 32**, 181 (1993);
B. Foster et al., Nucl. Inst. Meth. **A 338**, 254 (1994).

[10] M. Derrick et al., Nucl. Inst. Meth. **A 309**, 77 (1991);
A. Andresen et al., Nucl. Inst. Meth. **A 309**, 101 (1991);
A. Caldwell et al., Nucl. Inst. Meth. **A 321**, 356 (1992);
A. Bernstein et al., Nucl. Inst. Meth. **A 336**, 23 (1993).

[11] J. Andruszków et al., Preprint DESY-92-066, DESY, 1992;
ZEUS Coll., M. Derrick et al., Z. Phys. **C 63**, 391 (1994);
J. Andruszków et al., Acta Phys. Pol. **B 32**, 2025 (2001).

[12] ZEUS Coll., S. Chekanov et al., Phys. Lett. **B 547**, 164 (2002).

[13] H. Abramowicz, A. Caldwell and R. Sinkus, Nucl. Inst. Meth. **A 365**, 508 (1995);
R. Sinkus and T. Voss, Nucl. Inst. Meth. **A 391**, 360 (1997).

[14] S. Bentvelsen, J. Engelen and P. Kooijman, *Proc. of the Workshop on Physics at HERA*, W. Buchmüller and G. Ingelman (eds.), Vol. 1, p. 23. Hamburg, Germany, DESY (1992);
K.C. Höger, ibid., p. 43.

[15] S. Catani et al., Nucl. Phys. **B 406**, 187 (1993).

[16] S.D. Ellis and D.E. Soper, Phys. Rev. **D 48**, 3160 (1993).

[17] J.E. Huth et al., *Research Directions for the Decade. Proc. of Summer Study on High Energy Physics, 1990*, E.L. Berger (ed.), p. 134. World Scientific (1992). Also in preprint FERMILAB-CONF-90-249-E.

[18] R. Brun et al., GEANT3, Technical Report CERN-DD/EE/84-1, CERN, 1987.

[19] A. Kwiatkowski, H. Spiesberger and H.-J. Möhring, Comp. Phys. Comm. **69**, 155 (1992);
H. Spiesberger, *An Event Generator for ep Interactions at HERA Including Radiative Processes (Version 4.6)*, 1996, available on
`http://www.desy.de/~hspiesb/heracles.html`.

[20] K. Charcuła, G.A. Schuler and H. Spiesberger, Comp. Phys. Comm. **81**, 381 (1994);
H. Spiesberger, *HERACLES and DJANGOH: Event Generation for ep Interactions at HERA Including Radiative Processes*, 1998, available on
`http://www.desy.de/~hspiesb/djangoh.html`.

[21] Y. Azimov et al., Phys. Lett. **B 165**, 147 (1985);
G. Gustafson, Phys. Lett. **B 175**, 453 (1986);
G. Gustafson and U. Pettersson, Nucl. Phys. **B 306**, 746 (1988);
B. Andersson et al., Z. Phys. **C 43**, 625 (1989).

[22] L. Lönnblad, Comp. Phys. Comm. **71**, 15 (1992);
L. Lönnblad, Z. Phys. **C 65**, 285 (1995).

[23] G. Ingelman, A. Edin and J. Rathsman, Comp. Phys. Comm. **101**, 108 (1997).

[24] H.L. Lai et al., Eur. Phys. J. **C 12**, 375 (2000).

[25] B. Andersson et al., Phys. Rep. **97**, 31 (1983).

[26] T. Sjöstrand, Comp. Phys. Comm. **82**, 74 (1994);
T. Sjöstrand et al., Comp. Phys. Comm. **135**, 238 (2001).

[27] T. Sjöstrand, Comp. Phys. Comm. **39**, 347 (1986);
T. Sjöstrand and M. Bengtsson, Comp. Phys. Comm. **43**, 367 (1987).

[28] S. Catani and M.H. Seymour, Nucl. Phys. **B 485**, 291 (1997). Erratum in Nucl. Phys. **B 510**, 503 (1998).

[29] R.K. Ellis, D.A. Ross and A.E. Terrano, Nucl. Phys. **B 178**, 421 (1981).

[30] J. Pumplin et al., JHEP **0207**, 012 (2002);
D. Stump et al., JHEP **0310**, 046 (2003).

[31] ZEUS Coll., S. Chekanov et al., Phys. Lett. **B 531**, 9 (2002);
ZEUS Coll., S. Chekanov et al., Eur. Phys. J. **C 23**, 615 (2002);
M. Wing (on behalf of the ZEUS Coll.), *Proc. of the 10th International Conference on Calorimetry in High Energy Physics*, R. Zhu (ed.), p. 767. Pasadena, USA (2002). Also in preprint hep-ex/0206036.

[32] ZEUS Coll., S. Chekanov et al., Eur. Phys. J. **C 21**, 443 (2001).

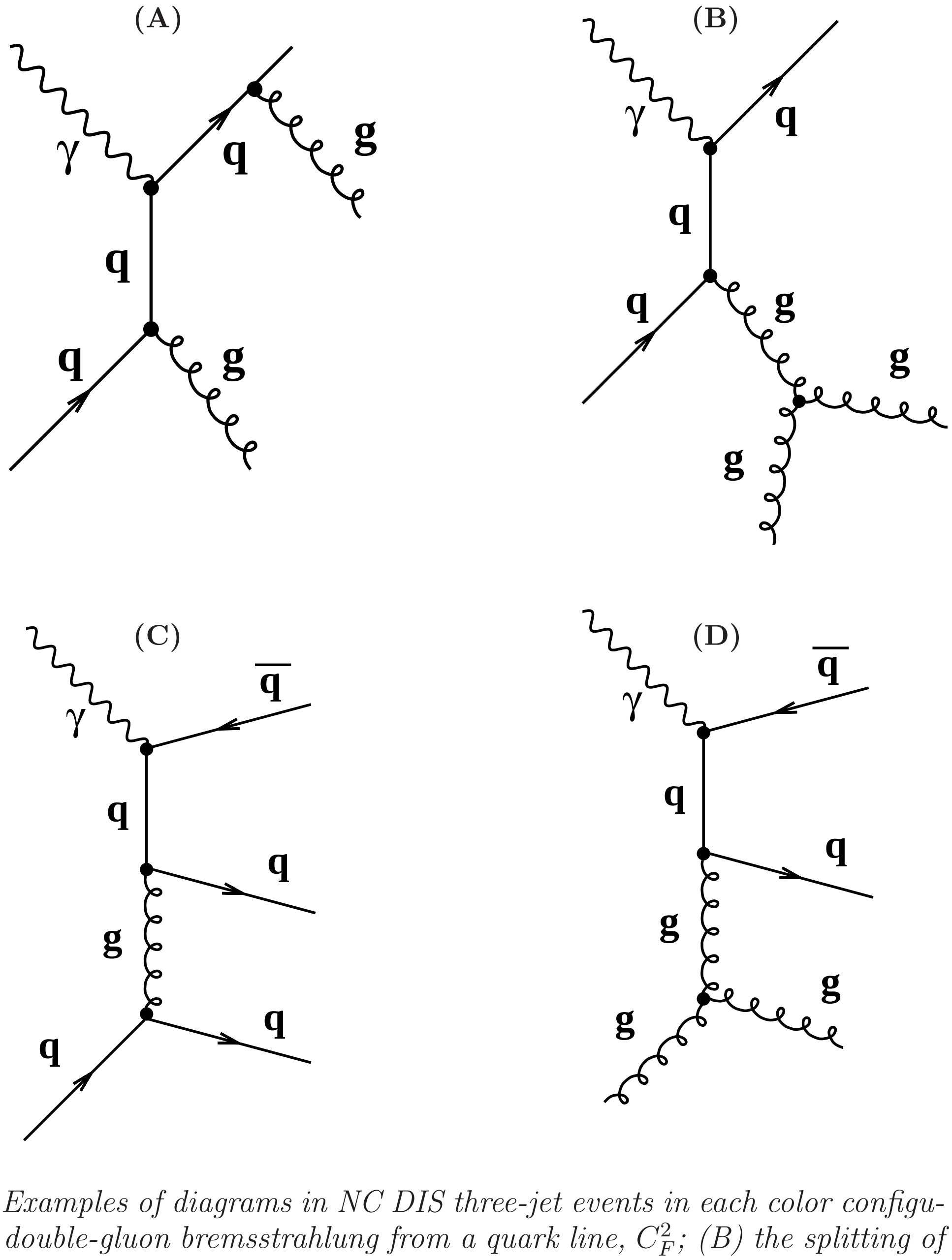

Figure 1: *Examples of diagrams in NC DIS three-jet events in each color configuration: (A) double-gluon bremsstrahlung from a quark line, C_F^2; (B) the splitting of a virtual gluon into a pair of final-state gluons, $C_F C_A$; (C) the production of a $q\bar{q}$ pair through the exchange of a virtual gluon emitted by an incoming quark, $C_F T_F$; (D) the production of a $q\bar{q}$ pair through the exchange of a virtual gluon arising from the splitting of an incoming gluon, $T_F C_A$.*

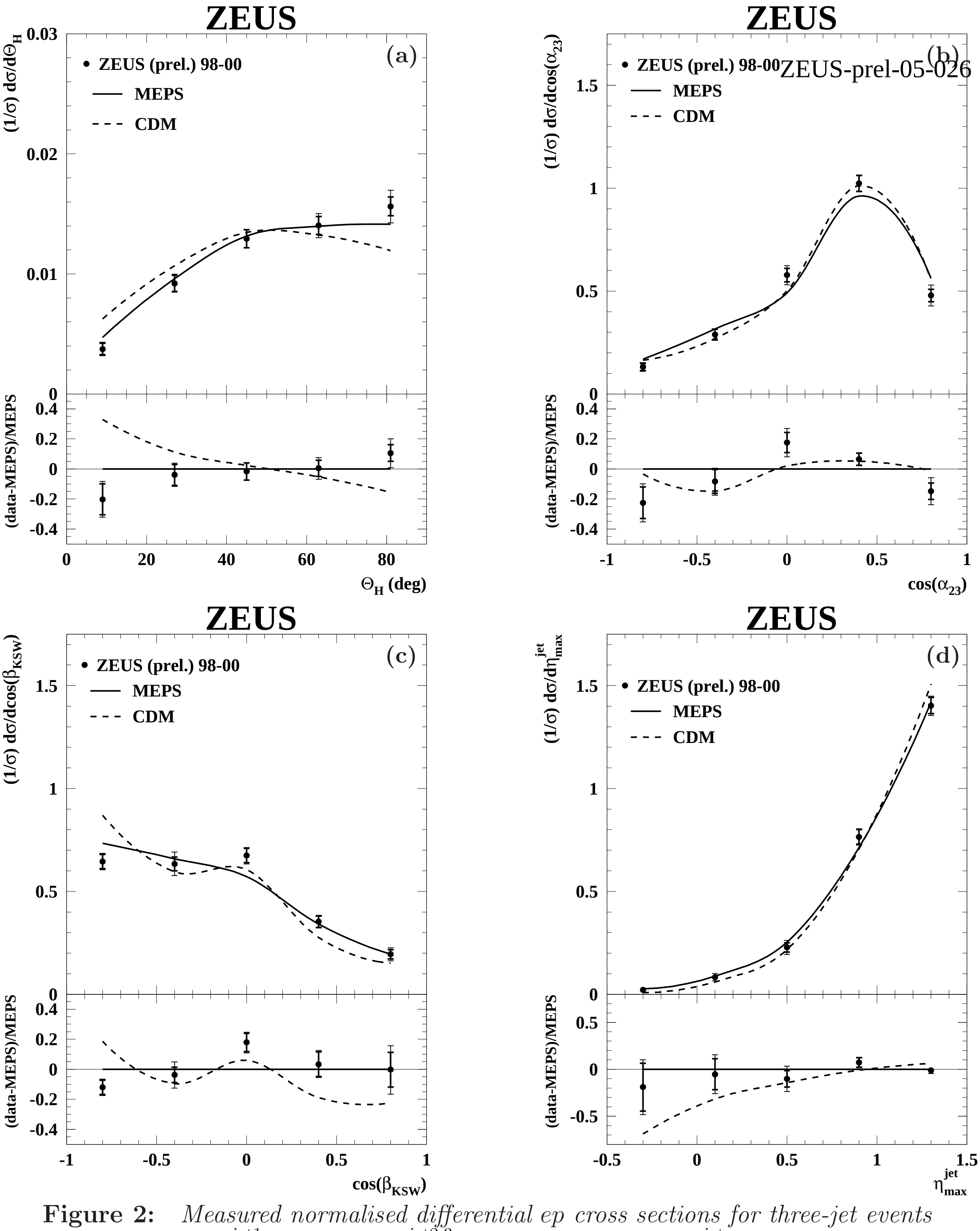

Figure 2: *Measured normalised differential ep cross sections for three-jet events in NC DIS for $E_{T,\mathrm{B}}^{\mathrm{jet1}} > 8$ GeV, $E_{T,\mathrm{B}}^{\mathrm{jet2,3}} > 5$ GeV and $-2 < \eta_{\mathrm{B}}^{\mathrm{jet}} < 1.5$ in the kinematic region defined by $Q^2 > 125$ GeV^2 and $|\cos\gamma_h| < 0.65$ as functions of (a) θ_H, (b) $\cos\alpha_{23}$, (c) $\cos\beta_{\mathrm{KSW}}$ and (d) $\eta_{\mathrm{max}}^{\mathrm{jet}}$ (dots). The thick error bars represent the statistical uncertainties of the data, and the thin error bars show the statistical and systematic uncertainties added in quadrature. For comparison, the predictions of leading-logarithm parton-shower Monte Carlo models of MEPS (solid lines) and CDM (dashed lines) are included. The lower part of the figures displays the fractional difference between the measured normalised cross section and the corresponding predictions of MEPS (dots); the fractional difference between the predictions of CDM and MEPS is also shown (dashed lines).*

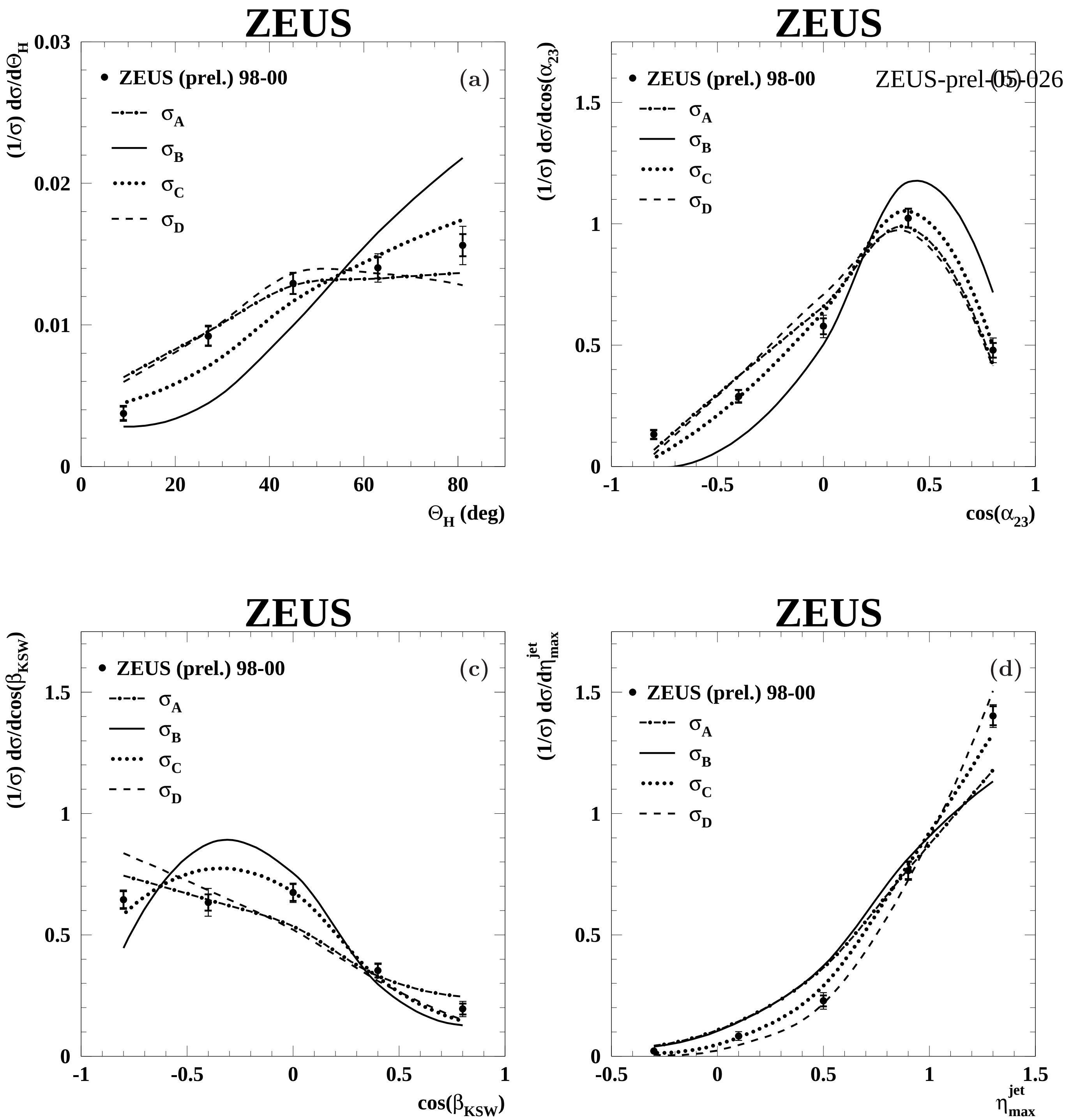

Figure 3: *Measured normalised differential ep cross sections for three-jet events in NC DIS for $E_{T,\mathrm{B}}^{\mathrm{jet1}} > 8$ GeV, $E_{T,\mathrm{B}}^{\mathrm{jet2,3}} > 5$ GeV and $-2 < \eta_{\mathrm{B}}^{\mathrm{jet}} < 1.5$ in the kinematic region defined by $Q^2 > 125$ GeV^2 and $|\cos\gamma_h| < 0.65$ as functions of (a) θ_H, (b) $\cos\alpha_{23}$, (c) $\cos\beta_{\mathrm{KSW}}$ and (d) $\eta_{\mathrm{max}}^{\mathrm{jet}}$ (dots). Other details as in the caption to Fig. 2. For comparison, the color components of the $\mathcal{O}(\alpha\alpha_s^2)$ calculations of* DISENT *(see text) are included.*

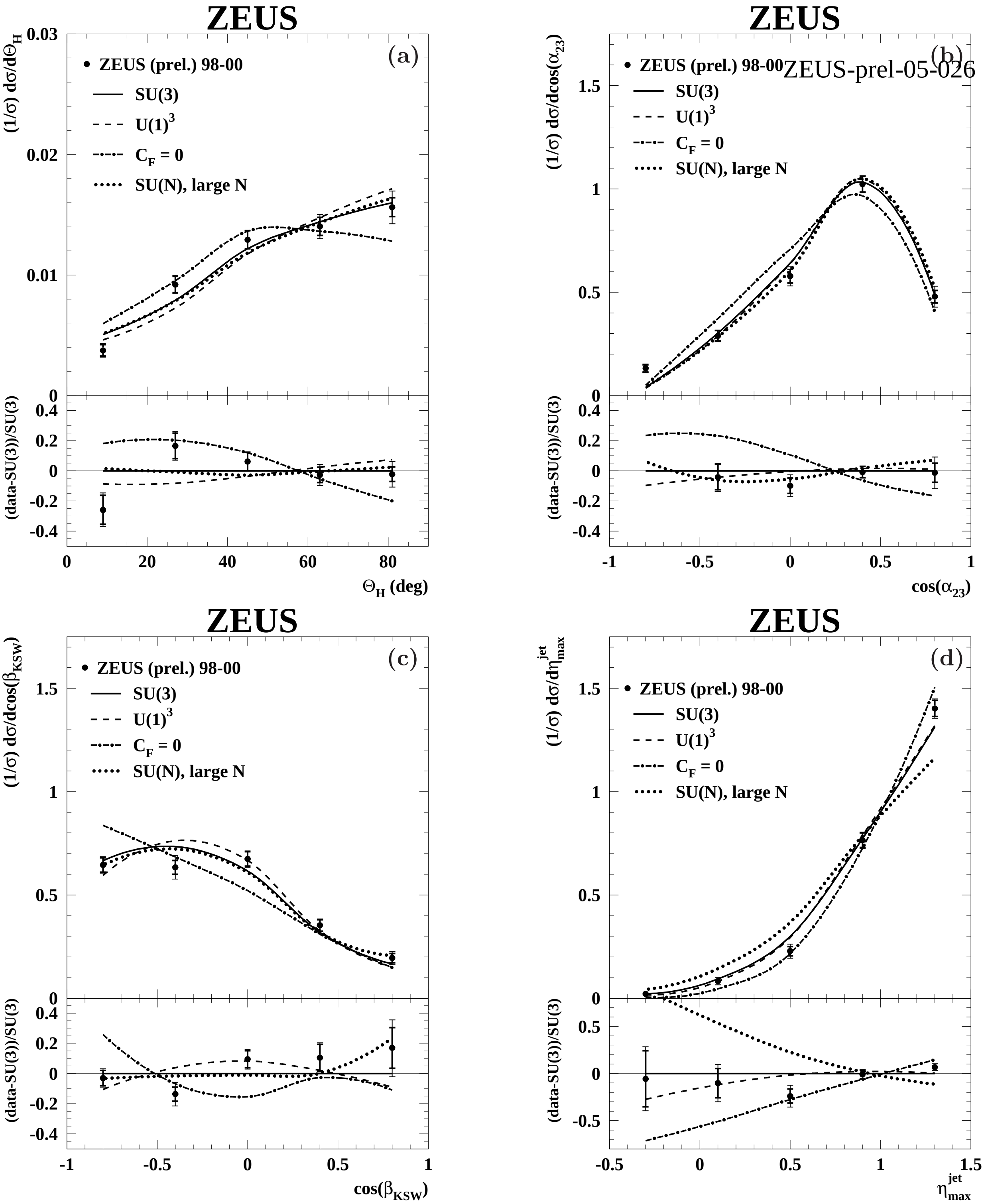

Figure 4: *Measured normalised differential ep cross sections for three-jet events in NC DIS for* $E_{T,\mathrm{B}}^{\mathrm{jet1}} > 8$ *GeV,* $E_{T,\mathrm{B}}^{\mathrm{jet2,3}} > 5$ *GeV and* $-2 < \eta_{\mathrm{B}}^{\mathrm{jet}} < 1.5$ *in the kinematic region defined by* $Q^2 > 125$ *GeV*^{2} *and* $|\cos\gamma_h| < 0.65$ *as functions of (a)* θ_H*, (b)* $\cos\alpha_{23}$*, (c)* $\cos\beta_{\mathrm{KSW}}$ *and (d)* $\eta_{\max}^{\mathrm{jet}}$ *(dots). Other details as in the caption to Fig. 2. For comparison, the* $\mathcal{O}(\alpha\alpha_s^2)$ *calculations of* DISENT *(see text) based on SU(3) (solid lines), U(1)*^{3} *(dashed lines), SU(N) in the limit of large N (dotted lines) and* $C_F = 0$ *(dot-dashed lines) are included. The lower part of the figures displays the fractional difference between the measured cross section and the calculation based on SU(3) (dots); the fractional difference between the predictions of U(1)*^{3} *(dashed lines),* $C_F = 0$ *(dot-dashed lines) or SU(N) in the limit of large N (dotted lines) and SU(3) are also shown.*